| Journal of Coastal Research | 24 | 6 | 1369–1378 | West Palm Beach, Florida | November 2008 |
|---|---|---|---|---|---|

# Aeolian Megaripples: Mathematical Model and Numerical Simulations

**Hezi Yizhaq**

Department of Solar Energy and Environmental Physics
The Jacob Blaustein Institutes for Desert Research (BIDR)
Ben-Gurion University of the Negev, Sede Boqer Campus 84990
Israel
yiyeh@bgu.ac.il

**ABSTRACT**

YIZHAQ, H., 2008. Aeolian megaripples: mathematical model and numerical simulations. *Journal of Coastal Research,* 24(6), 1369–1378. West Palm Beach (Florida), ISSN 0749-0208.

Aeolian sand ripples are a common feature on sandy deserts and beaches. Standard aeolian ripples have wavelengths of a few centimeters and amplitudes of a few millimeters. Sometimes, much larger ripples are observed. These are known by different names, such as ridges, granule ripples, gravel ripples, or megaripples. Aeolian megaripples are composed of a mixture of coarse and fine noncohesive material; a bimodal distribution of particle sizes is thought to be necessary for large, ripplelike bed forms to develop. Here, we discuss the extension of a recent model for the dynamics of aeolian megaripples. The model assumes that both the saltation and reptation fluxes are modulated by the emergent bed forms. We present a linear stability analysis of the full model as well as the results of numerical simulations. The modeled megaripples evolve through interactions between ripples of different sizes. The formation of megaripples is therefore another example of a self-organizing geomorphological system.

**ADDITIONAL INDEX WORDS:** *Aeolian sand ripples, megaripples, saltation, reptation, mathematical model, coarsening, numerical simulation.*

## INTRODUCTION

Aeolian ripples larger than those commonly found in fine sand (see Figure 1) are known in the literature by various names, such as ridges (Bagnold, 1941), granule ripples (Sharp, 1963), gravel ripples (Sakamoto-Arnold, 1988), or megaripples (Ellwood Evans, and Wilson, 1975). Large aeolian sand ripples on Earth have been described in many places: among them, the Kelso Dunes and Coachella Valley in southern California, by Sharp (1963); the Libyan desert, by Bagnold (1941) and El-Baz (1986); northern Sinai, by Tsoar (1990); Swakopmund, Namibia, by Fryberger, Hesp, and Hastings (1992); northeastern Iceland, by Mountney and Russell (2004); and the coastal dunes of northeastern Brazil (see Figure 1). Recently, enormous megaripples at Carachi Pampa, Argentina, at a height of 4000 m were documented by Milana (2005). These megaripples, composed of volcanic pebbles, were formed by the action of extremely strong winds (probably the strongest winds known on Earth ~400 km/h). Their wavelengths are up to 18 m, and their height is about 1.5 m.

There is a clear correlation between the ripple wavelength $\lambda$ and height $h$ (with a ripple index $\lambda/h$ of approximately 15), as well as between the wavelength and maximum particle size (see Figures 3 and 4 in Williams, Zimbelman, and Ward, 2002). According to Bagnold (1941), it may take decades or centuries to form huge megaripples, where their dimensions vary as the square root of age. Sharp (1963), however, suggested that with a large enough supply of coarse grains, it might take only weeks for well-defined granule ripples to form at Kelso Dunes. It was observed by Sakamoto-Arnold (1988) that during a severe windstorm in the southern San Joaquin Valley in California, megaripples formed on a timescale of hours or days. A bimodal distribution of particle sizes seems to be required for large, megaripple bed forms to develop, as Sharp (1963) found that coarse grains make up 50–80% of the crest material and less than 10–20% of the trough composition. Figure 2 shows a clear distinction between normal ripples and megaripples in a sand dune on the Jordanian side of the Araba Valley. It was found that the normal ripples were composed of fine grains alone, and the megaripples had coarse grains covering the crests and finer grains in the troughs. Megaripples form at the bottom of the dunes, the site of coarse-grain accumulation.

In wind tunnel experiments, protogranule ripples were found to drift downwind about 1 cm every 5 min (Fryberger, Hesp, and Hastings, 1992). Recent field experiments done by Brad Murray in Morocco (Murray, 2005) indicated that initial wavelength, as well as crest height, increases with wind speed. In addition, megaripple wavelength grows via a coarsening process similar to that occurring in normal ripples, in which ripple wavelength increases due to coalescence of smaller ripple (Murray, 2005). Table 1 summarizes the main characteristics of normal ripples and megaripples.

Interestingly enough, aeolian processes are extremely important for understanding the geology of Mars (Rubin, 2006). Images from the Mars Global Surveyor clearly portray dust

*DOI: 10.2112/08A-0012.1 received and accepted in revision 10 June 2008.*

Figure 1. Aeolian sand megaripples at Cearà coast in northeastern Brazil. The wavelength is more than 3 m (the length of the measure strip), and the height is about 50 cm. The diameter of the coarse grains that cover the ripple crest is about 3 mm. The average wind velocity during the dry season is 7.75 m/s (Jimenez *et al.,* 1999). Note that normal ripples (arrow) have developed at the troughs between the megaripples.

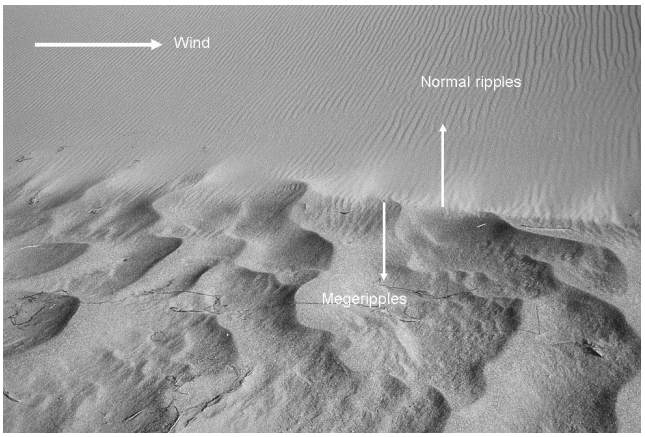


Figure 2. Clearly seen distinctions between normal and megaripples at Fidan Sand Dunes, Jordan (see Saqqa and Atallah [2004] for details). The normal ripples form on the windward slope of a linear dune and are composed only of fine grains. The megaripples exhibit profound spatial grain-size sorting. The coarse grains compose the crests, and finer grains generally cover the troughs. Note that normal ripples can be found also between the megaripples (arrow) and that the crests of the megaripples are more wavy than those of normal ripples.

storms, dust devil traces, dunes, and megaripples. Large ripplelike bed forms have been observed in numerous locations on the planet (Edgett, 2001; Greeley *et al.,* 2002; Williams, Zimbelman, and Ward, 2002; Wilson, Zimbelman, and Williams, 2003; Yizhaq, 2005). Various applications of sand ripple studies on Earth and Mars were recently reviewed by Rubin (2006).

In his seminal book, *The Physics of Blown Sand and Desert Dunes,* Bagnold (1941) was the first to attempt to explain the formation of megaripples. He pointed out that the essential difference between normal ripples and megaripples lies in the relative magnitudes of wind strength and crest-grain size. In the case of megaripples, the wind is not strong enough to cause the coarse particles to saltate. Bagnold (1941) specified the following conditions for megaripple formation: (i) availability of sufficient coarse grains with a diameter 3–7 times greater than the mean diameter of the grains in saltation; (ii) a constant supply of fine sand in saltation to sustain forward motion of reptating (creeping or slipping) coarse grains; and (iii) wind velocity below the threshold that would drive coarse grains from the megaripple crest. His theory specifies that megaripples will grow indefinitely as long as the supply of fine particles continues.

Bagnold also described a strong-wind situation in which coarse grains can be driven into saltation, where megaripples break down into normal ripples. Sharp (1963), in his field research in Kelso Dunes and Coachella Valley, California, confirmed Bagnold's idea of megaripple formation but indicated that the principle of characteristic grain path is probably not applicable to the wavelength of megaripples. Sharp suggested that most of the considerations pertaining to normal ripples, including impact slope, shadow slope, height, and mean impact angle of saltating grains, can be applied to megaripples. Sharp showed that a concentration of larger grains capable of covering at least 50% of the crest surface is required for producing well-developed megaripples. He also noted that megaripples form slowly and move slowly and have considerable longevity compared to sand ripples.

In a carefully designed experiment in a 30-m-long wind tunnel, Walker (1981) showed that normal ripple spacing and height increase with increasing grain diameter and with sorting (the segregation of similarly sized sediments that naturally occurs during aeolian transport and deposition). He argued that although flow separation does not occur over aeolian ripples, something analogous develops. When the ripple grows high enough, it casts a "shadow" that shelters the ripple's lee slope from saltation bombardment, and Walker felt that this shadow zone might be important for megaripple formation. Based upon experiments with poorly sorted sands, he suggested that the concentration of coarse grains at the crest allows the ripple to continue growing higher at a given value of wind-shear stress. He derived this from the fact that coarse grains are harder to dislodge by saltating fine grains, and they are also more resistant to direct wind shear.

Table 1. *Main features of normal aeolian ripples and megaripples.*

| | Normal Ripples | Megaripples |
|---|---|---|
| Wavelength | Up to 30 cm | 30 cm–20 m |
| Ripple index (wavelength/height) | >15 (Sharp, 1963) | <15 (Sharp, 1963) |
| Timescale | Minutes (Anderson, 1990) | Days (Sakamoto-Arnold, 1988) and years (Bagnold, 1941) |
| Sorting | Unimodal distribution of grain sizes (typically 0.06 to 0.5 mm in diameter) | Bimodal distribution of grain sizes with coarse grains (1–4 mm in diameter) |

Fryberger, Hesp, and Hastings (1992) performed a series of experiments in a portable wind tunnel with sand that was collected from megaripples at Great Sand Dunes National Park, Colorado. In one experiment that started with a flat bed, they observed after 3 h of saltation that small megaripples ("proto"-granule ripples) formed, which migrated downwind. One hour later, megaripple growth was saturated, and they continued to migrate downwind. Unfortunately, the data on wind strength and ripple spacing were missing.

Tsoar (1990) studied the surface grain-size distribution between the crests and troughs of megaripples with wavelength of 25 cm and longer that formed on the plinth of a desert seif dune in the northern Sinai. He used a unique sampling technique in which the surfaces of the ripple crest and trough were individually sprayed with an adhesive. Following treatment with solvent to dissolve the glue, dispersion of the particles with a high-intensity sonic processor, washing, and drying, the samples were analyzed using standard sieves. Grain size of the megaripple particles was shown to be trimodal: one prominent coarse-grain mode and two small fine-grain modes. The amount of coarse grain decreased with distance below the ripple surface and almost disappeared at a depth several centimeters.

In contrast to Williams, Zimbelman, and Ward (2002), who studied large megaripples at Edwards and at Great Sand Dunes National Monument, Tsoar found that the wavelengths of megaripples were not significantly correlated with the mean crest- or surface-grain size or with the mean size of grains in the entire megaripple. This difference might be explained by the fact that Tsoar sampled megaripples with wavelengths between 25 and 50 cm, which can be considered nonrepresentative small megaripples. Moreover, he examined correlations with respect to mean grain size alone, but a correlation might have been found if he had examined wavelength *vs.* maximum grain size, as was observed by Williams, Zimbelman, and Ward (2002). Interestingly, Tsoar also concluded that no continuity existed between the wavelength of normal ripples and megaripples with increasing mean grain size. The question of continuity was also addressed by Ellwood, Evans, and Wilson (1975, their Figure 7c), who analyzed 120 samples and found that there was no discontinuity in the plot of the coarse twenty-percentile grain size ($P_{20}$) between ripples and megaripples. They concluded, therefore, that ripples and megaripples were formed by the same mechanism. This disagreement between Tsoar and Ellwood *et al.* may derive from the large number of samples taken by Ellwood, which covered many more wavelengths.

In recent work at the White Sands National Monument, New Mexico, Jerolmack and coworkers (Jerolmack *et al.,* 2006) measured the sand flux of coarse-grained ripples with wavelengths between 0.5 and 1 m and heights of 10 mm. They found that the small particles (0.1 mm to 1 mm) were transported by saltation and that coarse grains (1 mm to 3 mm) were transported by surface creep. They observed clear spatial segregation between the two populations of grains. The coarse grains were concentrated on the crests, while troughs contained few coarse grains. This is the first field experiment that supports Bagnold and Elwood's hypotheses of megaripple formation where coarse grains are transported solely by reptation. However, the relatively small, 10-mm-high coarse ripples they studied should be classified as atypical, shallow megaripples.

## MATHEMATICAL MODELS

Although models of the dynamics of standard aeolian ripples have been developed (see, *e.g.,* Yizhaq, Balmforth, and Provenzale, 2004), the mathematical description of megaripple evolution has received little attention. The work of Ellwood, Evans, and Wilson (1975), is built on data taken from 120 samples collected from sand ripples in the Algerian Sahara. Their approach was based on the assumption that megaripple wavelength is dictated mainly by the mean saltation length of fine particles bouncing off coarse particles in sands with a bimodal particle distribution. By using an experimentally determined "rebound probability matrix," they calculated the grain jump of various sizes of grains bouncing of beds of different-sized grains in winds of different shear velocities. Their numerical calculations showed an entire range of saltation lengths, which they related to the range of observed megaripple wavelengths.

They presented two scenarios for megaripples formation in sand having a bimodal mixture of two grain sizes. The first was termed "fine fraction impact ripple formation," in which the wind strength is insufficient to dislodge the coarse grains. Here, the ripple wavelength should correspond to the mean saltation length of the fine grains. In the second case, which they termed "coarse fraction impact ripple formation," the wind is strong enough to saltate the coarse grains, and the ripple wavelength should correspond to the mean saltation path of the coarse grains. There are several drawbacks of their model: (i) neither the saltation-induced motion of grains in the bed nor the creeping of grains along the surface, *i.e.,* reptation (Anderson, 1987), was explicitly taken into consideration; (ii) their extended "characteristic length" idea, following Bagnold, rules out the coarsening mechanism that seems to operate in megaripple formation (Murray, 2005); (iii) they did not present any one-to-one comparison of their calculated wavelengths with field-measured ripple wavelength; and (iv) they completely ignored the effect of ripple height (which grows during megaripple evolution) on spacing (Sharp, 1963; Walker, 1981).

The segregation mechanism operating in regular aeolian sand ripples was modeled by Anderson and Bunas (1993). They proposed a cellular automata approach, which uses discrete space and time functions for numerical evaluations to model a sand bed composed of two grain sizes. The bed was subjected to impacts of saltating grains that rebounded and ejected other grains according to rules derived from a model of the dynamics of individual granular impacts. The basic mechanism for the vertical sorting of grain size was the differential hop-length (reptation length) effect. Numerical simulations of the model showed that the coarsened crests appear only after the ripples have reached significant heights, namely, when the lee slopes are strongly shadowed from impacts. Anderson and Bunas concluded that on a mature ripple, coarse grains could not leap far enough down the lee side to escape the shadow zone. Coarse grains would then be bur-

ied by subsequent deposition on the lee face and reemerge as the ripple drifted downwind. Although they did not address megaripple formation specifically, their findings can be strongly related to its initial stage, namely, the sorting process that allows the vertical growth of ripples.

Particle-size segregation in normal sand ripples was also modeled by Ouchi and Nishimori (1995) using the cellular automata approach. They concluded that the most effective factor for grain segregation is the difference in creep dynamics (*i.e.,* reptation) of different-sized grains, which depends on the inner friction and inertia of the grain. In their model, the surface creep dynamics were modeled by the slope; a grain falls down to a neighboring site once the slope exceeds some critical angle, which is larger for the heavy grain. According to their model, the grains are sorted by size because of the difference in the grain stability against external force. Sand grains move from the most unstable place (crest) to the most stable place (trough). The coarse grains, which are heavier, are relatively more stable and tend to preferentially accumulate at the ripple crest.

A simple mathematical model of aeolian megaripples was recently introduced by Yizhaq (2004); this model is based on the Anderson model (Anderson, 1987) and on the mechanism of "fine-fraction impact ripples." It is built around the assumption that the particles consist of a mixture of sand grains of two different sizes and that the wind is not powerful enough to saltate the coarse fraction. This simplified model takes into account both saltation and reptation fluxes as given in the Exner equation (Anderson, 1987), which expresses the conservation of mass. Spatial variability of the saltation flux is due to sufficiently large undulations of the bed. Here, the saltation flux can depend on bed topography, as well as on the spatial variability of the flux of saltating grains. Variability of the saltation flux leads to a space-time dependence of the number density of impacting grains on a flat surface, which adds a new level of complexity to the solution because it modifies the number of reptation particles.

In the model presented here, I modify the reptation flux due to changes of the impact intensity of saltating grains and present numerical solutions. This is a two-scale model in which spatial variations of the saltation flux dominate at large scales (order of meters) and for long times, while spatial variations of the reptation flux dominate on small scales (order of centimeters) and for shorter timescales. Linear stability analysis indicates the presence of two maxima in the growth rates of the unstable modes. One corresponds to megaripples and the other to normal ripples.

The starting point is the one-dimensional Exner equation,

$$\zeta_t = -\frac{1}{\rho_p(1-\lambda_p)}\frac{\partial Q}{\partial x}, \tag{1}$$

where $\zeta(x, t)$ is the local height of the bed surface at point $x$ and time $t$, $\rho_p$ is the density of a sand grain, and $\lambda_p$ is the porosity of the bed (typically taken as 0.35). $Q(x, t)$ is the horizontal flux of sand grains mobilized by wind action (sediment mass per unit width per unit time). According to the Exner equation, erosion (or deposition) occurs in regions where the sediment flux is diverging (or converging), and there is no change in surface height and the transport rate is spatially uniform. Experimental results (Anderson, 1987) indicate that the bombardment process generates two populations of moving grains: the first is composed of grains that are ejected with large energy and are accelerated by the wind to form the population of "saltating grains" (or "saltons"). The second population consists of low-energy ejected grains that stay close to the sand surface, forming the so-called "reptating population" ("reptons"). The total sand flux is then the sum of the saltation and the reptation fluxes,

$$Q = Q_s + Q_r. \tag{2}$$

We assume that there is no alternation in particle movement; the fine grains move only by saltation, and the coarse grains only by reptation. This results from the difference in particle sizes of the two populations and the assumption that the wind speed is below that of the fluid threshold of the coarse particles. In the Exner equation (Equation 1), spatial variability of the sand flux is the single factor that determines surface evolution. For normal aeolian sand ripples, we assume that the ballistic, wind-buffeted trajectory of the saltating particle occurs in a manner that is essentially independent of jump length, namely, that its impact angle will not vary significantly over a broad range of saltation lengths (Anderson, 1987). As a result, the model assumes that all saltating grains descend at a fixed angle and with a fixed speed. For this case, only the spatial variability of the reptation flux enters into the Exner equation (Yizhaq, Balmforth, and Provenzale, 2004). This hypothesis is correct only when bed undulations have a wavelength much smaller than the mean saltation jump. For standard sand ripples, typical wavelengths are about 10–15 cm, and typical saltation lengths are about 50 cm. Thus, neglecting the spatial variability of the saltation flux is justified (Anderson, 1987, 1990; Misbah and Valance, 2003). This assumption of uniform saltation flux is not valid for bed forms with large wavelengths, such as megaripples. In this case, both saltation and reptation fluxes affect the evolution of the sand surface.

Yizhaq (2004) modeled the dynamics of a sediment surface consisting of a mixture of sand grains with two different sizes, coarse ($c$) and fine ($f$). For this bimodal distribution, the horizontal saltation flux can be written as $Q_s = Q_{sf} + Q_{sc}$, where $Q_{sf}$ ($Q_{sc}$) is the saltation flux of fine (coarse) particles. Similarly, the reptation flux $Q_r$ can be written as $Q_r = Q_{rc} + Q_{rf}$, and the total flux becomes

$$Q = Q_{sf} + Q_{sc} + Q_{rc} + Q_{rf}. \tag{3}$$

Consistent with observations, two basic simplifications were introduced into the model. First, it was assumed that the wind is not strong enough to drive coarse particles into saltation, *i.e.,* $Q_{sc} = 0$. Second, the reptation flux of fine grains is neglected ($Q_{rf} = 0$), as it provides only a small contribution to the total sand flux due to the armoring effect of the coarse particles (Fryberger, Hesp, and Hastings, 1992; Sarre and Chancey, 1990; Tsoar, 1990). This contribution, however, may be important for initial times, where the ripples are small and the segregation between coarse and fine particles is not prominent.

The next step requires a quantitative expression of the saltation flux of the fine grains and the reptation flux of the

coarse grains. Following Anderson (1987) and Yizhaq (2004), the saltation flux of the fine particles can be written as

$$Q_{sf}(x) = m_f(1 - \mu_s\zeta_x)\int_{-\infty}^{\infty} p_{sf}(\beta)\, d\beta \int_{x-\beta}^{x} N_{im}(x')\, dx', \quad (4)$$

where $p_{sf}(\beta) = A\exp[-(\beta - b)/(2\sigma^2)]$, the probability distribution of the saltation lengths ($\beta$), is taken as a normal distribution (Anderson and Haff, 1988), $b$, the mean saltation length, is defined as $b = \int_{-\infty}^{\infty} p_{sf}(\beta)\beta\, d\beta$, and $\sigma$ is the standard deviation. $A$ is defined as $A = 1/(\sigma\sqrt{2}\pi)$ to ensure that $\int_{-\infty}^{\infty} p_{sf}(\beta)\, d\beta = 1$; $m_f$ is the mass of a fine grain; and $\mu_s$ is a phenomenological parameter that takes into account the dependence of saltation flux on bed slope. It was assumed that the flux decreases on the windward slope and increases on the lee slope. Consistent with observations (Anderson and Sørensen, 1991), it was also assumed that, on average, only one saltating grain is ejected per each impacting grain. Note that according to Equation 4, the saltation flux is not uniform in space and therefore contributes to ripple evolution.

The number density (impact rate) of saltating particles, $N_s$, that hit the surface per unit area per unit time is given by

$$N_s(x) = \frac{\cot\phi N_{im}^0}{b}\int_{-\infty}^{\infty} p_{sf}(\beta)\, d\beta \int_{x-\beta}^{x} \frac{\tan\phi + \zeta_{x'}}{\sqrt{1 + \zeta_{x'}^2}}\, dx', \quad (5)$$

where $N_{im}^0$ is the number density of impacting grains on the flat surface, $\zeta_x = \tan\theta$ is the bed inclination (positive at the windward slope), and $\varphi$ is the impact angle. For standard aeolian sand ripples, the saltation flux on a flat surface is assumed to be uniform, and $N_{im}^0$ is therefore constant (the flux probably also depends on wind strength). However, for the case of megaripples, the assumption of saltation flux uniformity is not valid, leading to a more complex space-time dependence of $N_{im}(x, t)$. Note that for $3_x = \theta$ (*i.e.,* the flat bed), $N_s(x) = N_{im}^0$. In the context of normal ripples, the model of Nishimori-Ouchi (1993) takes into account the spatial variability of the saltation flux due to deformation of the bed. For normal ripples, which have a small wavelength compared to the mean saltation jump, this might be negligible, but for megaripples, which are larger bed forms, it may be important.

Similarly, reptation flux is written as

$$Q_{rc} = m_c n_p N_s(x)(1 - \mu_r\zeta_x)\int_0^{\infty} p_{rc}(\alpha)\, d\alpha \int_{x-\alpha}^{x} \frac{\tan\phi + \zeta_{x'}}{\sqrt{1 + \zeta_{x'}^2}}\, dx' \quad (6)$$

where $p_{rc}(\alpha)$ is the so-called "splash function," which describes the distribution of the reptation lengths and is assumed to have an exponential distribution (Anderson, 1987; Anderson and Haff, 1988), $p_{rc}(\alpha) = e^{-\alpha/a}/a$, where $a$ is the mean reptation length defined as $a = \int_0^{\infty} \alpha p_{rc}(\alpha)\, d\alpha$ and $\int_0^{\infty} p_{rc}(\alpha)\, d\alpha = 1$, $m_c$ is the mass of a coarse grain, and $n_p$ is the average number of reptons ejected by impact of one fine saltating grain. The parameter $\mu_r$ includes bed-slope modifications of the ballistic trajectory (Prigozhin, 1999); the magnitude of $\mu_r$ must be determined empirically, but it is related to the angle at which the reptating grain is ejected (Yizhaq, 2004).

By substituting the expressions for the saltation and reptation fluxes into the Exner equation, we get the following expression, which is more complex than the version previously presented by Yizhaq (2004),

$$\frac{\partial\zeta}{\partial t} = -Q_0\partial_x\left[(1 - \mu_s\zeta_x)\int_{-\infty}^{\infty} p_{sf}(\beta)\, d\beta \int_{x-\beta}^{x} F(x')\, dx'\right] - \frac{Q_0\delta n_p\cot\phi}{b}\partial_x \times\left\{(1 - \mu_s\zeta_x)(1 - \mu_r\zeta_x)\left[\int_{-\infty}^{\infty} p_{sf}(\beta)\, d\beta \int_{x-\beta}^{x} F(x')\, dx'\right] \times\left[\int_0^{\infty} p_{rc}(\alpha)\, d\alpha \int_{x-\alpha}^{\varepsilon} F(x')\, dx'\right]\right\}. \quad (7)$$

Here $Q_0 = N_{im}^0 m_f\cot\phi/[\rho_p(1 - \lambda_p)]$ and

$$F(x) = \frac{\mathrm{Max}(\tan\phi + \zeta_x, 0)}{\sqrt{1 + \zeta_x^2}}, \quad (8)$$

which represents a local shadowing effect that takes on a value of 0 when the ripple slope exceeds the impact angle. This factor was added to avoid the nonoccurring negative flux predicted by the simplified model for a lee slope angle exceeding the impact angle $\varphi$; $\delta = m_c/m_f = (D_c/D_f)^3$, where $D_c$ and $D_f$ are the diameters of the coarse and the fine grains, respectively, assuming identical density and ideal spherical shape. According to Bagnold (1941), a saltation grain can sustain the forward movement of a coarse grain with a diameter 3–7 times larger than its own diameter, leading to $27 \le \delta \le 343$. Table 2 summarizes the parameters used in the model.

Table 2. *Definitions of the major model parameters.*

| Symbol | Definitions of the Parameters |
|---|---|
| $a$ | Mean reptation length |
| $A$ | Normalization constant ($A = 1/\sigma\sqrt{2\pi}$) |
| $b$ | Mean saltation length |
| $m_f$ | Fine grain mass |
| $m_c$ | Coarse grain mass |
| $n_p$ | Number of ejecting coarse grains per saltation impact |
| $N_m$ | Number density of impacting grains on an inclined surface |
| $N_{im}^0$ | Number density of impacting grains on a flat surface ($\sim 10^7$ $m^{-2}$ $s^{-1}$) |
| $p_{rc}$ | Probability distribution of coarse reptating grains (taken as exponential) |
| $p_{sf}$ | Probability distribution of fine saltating grains (taken as normal Gaussian) |
| $\alpha$ | Reptation jump length |
| $\beta$ | Saltation jump length |
| $\sigma$ | Standard deviation of $p_{sf}$ |
| $\lambda_p$ | Bed porosity (typically taken as 0.35) |
| $\delta$ | $m_f/m_c$ ($27 \le \delta \le 343$) |
| $\theta$ | Bed inclination |
| $\varphi$ | Descending angle of saltation grains |
| $\mu_r$ | Reptation length modification coefficient due to bed slope |
| $\mu_s$ | Saltation length modification coefficient due to bed slope |

A linear stability analysis of small bed perturbations is carried out by inserting an infinitesimal sinusoidal perturbation into Equation 7, given by

$$\zeta(x, t) = \zeta_0\exp[ik(x - ct)], \quad (9)$$

where $\zeta_0$ is the perturbation amplitude, and $k$ is the wavenumber ($k = 2\pi/\kappa$), and by neglecting higher orders terms (for example, using $F(x) \approx \tan\varphi + \zeta_x$). The phase speed, $c$, is a complex number $c = c_r + ic_i$; thus the perturbation (Equation 9) can be written as:

$$\zeta(x, t) = \zeta_0 \exp(kc_i t)\exp ik(x - c_r t). \quad (10)$$

Equation 10 indicates that $c_i$ denotes the perturbation growth rate, whereas $c_r$ denotes its translation speed.

Equation 7 can be written (after doing the spatial differentiation) in the following way:

$$\frac{\partial\zeta}{\partial t} = Q_0\left\{\mu_s\zeta_{xx}\int_{-\infty}^{\infty} p_{sf}(\beta)\,d\beta\int_{x-\beta}^{x} F(x')\,dx' + (1 - \mu_s\zeta_x) \times \int_{-\infty}^{\infty} p_{sf}(\beta)[F(x - \beta) - F(x)]\,d\beta\right\} + \frac{Q_0\delta n_p \cot\phi}{b}\Bigg[[\mu_s\zeta_{xx}(1 - \mu_r\zeta_x)B_1B_2] + [\mu_r\zeta_{xx}(1 - \mu_s\zeta_x)B_1B_2] + (1 - \mu_s\zeta_x)(1 - \mu_r\zeta_x) \times \left\{\int_{-\infty}^{\infty} p_{sf}(\beta)[F(x - \beta) - F(x)]\,d\beta\right\}B_1 + (1 - \mu_s\zeta_x)(1 - \mu_r\zeta_x) \times \left\{\int_{0}^{\infty} p_{rc}(\alpha)[F(x - \alpha) - F(x)]\,d\alpha\right\}B_1\Bigg], \quad (11)$$

where

$$B_1 = \int_{-\infty}^{\infty} p_{sf}(\beta)\,d\beta\int_{x-\beta}^{x} F(x')\,dx' \quad \text{and}$$

$$B_2 = \int_{0}^{\infty} p_{rc}(\alpha)\,d\alpha\int_{x-\alpha}^{x} F(x')\,dx'.$$

If we follow the calculation given by Yizhaq *et al.* (2004) and use the following expressions:

$$\frac{\partial\zeta}{\partial x} = i\zeta_0 k\,\exp ik(x - ct),$$

$$\frac{\partial^2\zeta}{\partial x^2} = -\zeta_0 k^2 \exp ik(x - ct),$$

$$\frac{\partial\zeta}{\partial t} = -ikc\zeta_0 \exp ik(x - ct),$$

$$\zeta(x) - \zeta(x - \alpha) = \zeta_0[1 - \exp(-ik\alpha)]\exp ik(x - ct),$$

$$\hat{p}_{sf}(k) \equiv \int_{-\infty}^{\infty} p_{sf}(\beta)\exp(-ik\beta)\,d\beta = \exp\left(-\frac{k^2\sigma^2}{2}\right) - ibk,$$

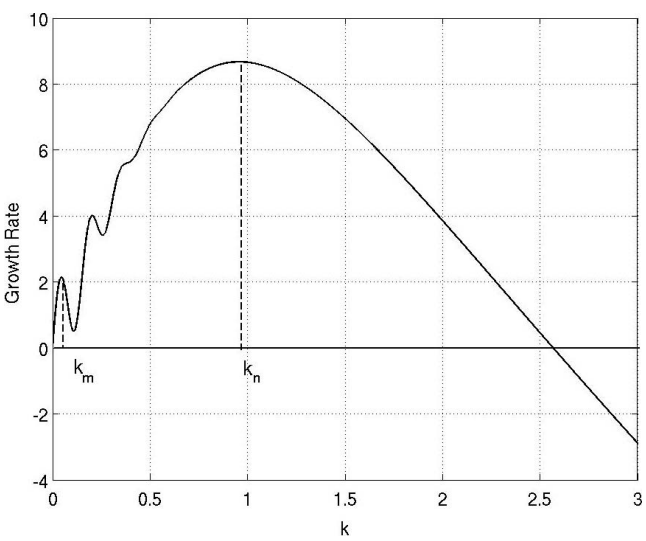


Figure 3. Dispersion curves showing the perturbation growth rate *vs.* wavenumber ($k = 2\pi/\lambda$) for infinitesimal perturbations as given in Equation 14. The first maximum, $k_m$, represents ripples with $\lambda = 138$ cm; the second maximum, $k_n$, represents ripples with $\lambda = 30.95$ cm; and the global maximum represents ripples with $\lambda = 6.614$ cm. Parameters: $b = 0.4$ m, $a = 0.0075$ m, $\sigma = 0.05$ m, $\mu_r = 0.4$, $\mu_s = 0.4$, $\delta = 27$, $\varphi = 10^0$, $n_p = 1$.

$$\hat{p}_{rc}(k) \equiv \int_{-\infty}^{\infty} p_{rc}(\alpha)\exp(-ik\alpha)\,d\alpha = \frac{a^{-2}}{k^2 + a^{-2}} - \frac{ika^{-1}}{k^2 + a^{-2}}, \quad (12)$$

we get

$$c = Q_0(1 - \hat{p}_{sf}(k) - ik\mu_s b\tan\phi) + \frac{Q_o n_p\delta}{b}\{[1 - \hat{p}_{sf}(k) - ik\mu_s b\tan\phi]a + [1 - \hat{p}_{rc}(k) - ik\mu_r a\tan\phi]b\}. \quad (13)$$

Linear stability occurs for $c_i > 0$ (the imaginary part of $c$), where

$$\frac{c_i}{Q_0} = k\left[\frac{n_P\delta a^{-1}}{k_2 + a^{-2}} - \tan\phi(\delta n_r\mu_r a + \mu_s b + \mu_s a)\right] + \exp\left(-\frac{1}{2}\sigma^2k^2\right)\sin bk\left(1 + \frac{n_r\delta a}{b}\right). \quad (14)$$

Figure 3 shows growth curves representing two maxima, $k_n$ and $k_m$, corresponding to normal ripple and megaripple modes.

## NUMERICAL RESULTS

The model equations (Equations 7 and 8) were solved numerically using an explicit second-order finite-difference scheme with periodic boundary conditions on a SGI Altix 3700 super cluster (with 24 Itanium 2 processors). The integral terms were computed using the composite trapezoid rule, and the time integration was carried out using the second-

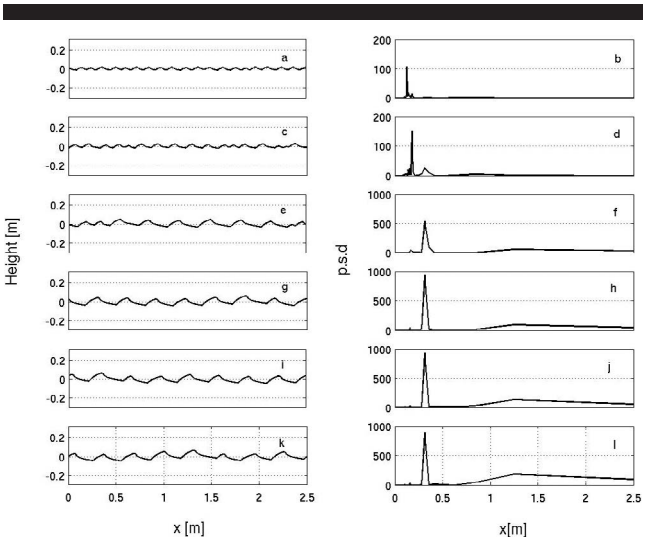


Figure 4. Ripple profiles calculated from the model equations (Equations 7 and 8) with $\mu_s = 0.4$. Heights *vs.* distance given at times: 2, 4, 8, 16, 22, 28 min (panels a, c, e, g, i, k, respectively), along with the corresponding power spectrum densities (panels b, d, f, h, j, l). The megaripples start off as normal ripples with different wavelengths, which can be seen to coalesce to form larger ripples. The initial conditions are random perturbations of a flat bed with periodic boundary conditions. The parameters are the same as for Figure 3 with $\mu_s = 0.4$. After 22 min, the wavelength is 31.25 cm, and the mean height is 7 cm. Ripple evolution is very slow.

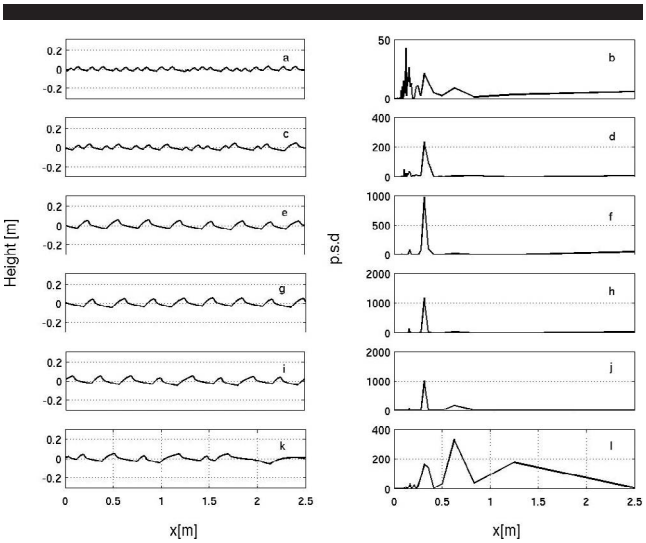


Figure 5. Ripple profiles calculated from the model equation (Equations 7 and 8) with $\mu_s = 0.2$. Heights *vs.* distance given at times: 2, 4, 8, 12, 20, 41 min (panels a, c, e, g, i, k, respectively), along with the corresponding power spectrum densities (panels b, d, f, h, j, l). All parameters are the same as in the previous figures except for $\mu_s = 0.2$. After 41 min, the ripple mean wavelength is $\lambda = 62.5$ cm. At later times, it is expected that the dominant mode will be the one with $\lambda = 125$ cm.

order Adams-Bashforth rule (Fausett, 1999). The grid was composed of 2048 points for a spatial dimension of 2.5 m (*i.e.,* spatial resolution of 1.22 mm) and a time step of 0.002 s. Because of the integral terms in Equation 7 and the large number of grid points, the computation time was large, and three days were needed to simulate 2 min of ripple evolution. Figure 4 shows the ripple cross section for $\mu_s = 0.4$, along with the corresponding power spectrum density (the mean of the Fourier transform squared amplitudes). After 32 min (which took 48 computing days), the ripple wavelength is 31.25 cm, and the next growing mode of 1.25 m develops very slowly, indicating a prolonged coarsening process.

Figure 5 shows the same growth pattern for $\mu_s = 0.2$. The ripples are higher, and after 41 min, the mode with $\lambda = 62.5$ cm dominates. The ripple cross section has the correct shape, with a convex stoss slope and concave lee slope.

These results agree with Murray's preliminary field observation in Morocco (Murray, 2005). He observed on smoothed plots that normal ripples and megaripples start with the same initial wavelength, on the order of centimeters, but after one day of strong wind, megaripples of 1 m wavelengths can develop. Figure 6 shows numerical results of ripple evolution during the first 8 min. After 8 min, the ripples mean wavelength is 35.71 cm, and their mean height is 10.18 cm.

The question of wavelength saturation is still open, as we need additional computation time to clarify this problem. In wind tunnel experiments, Andreotti, Claudin, and Pouliquen (2006) found that for normal ripples, the wavelength and the amplitude stopped growing, but no such observation exists for megaripples.

Evolution of the ripple mean height is shown in Figure 7 for $\mu_s = 0.4$ (circles) and $\mu_s = 0.2$ (squares). After initial linear growth, ripple height develops very slowly—the lower the value of $\mu_s$, the higher the ripples. At later times, the coarsening process for $\mu_s = 0.2$ is characterized by a decrease in

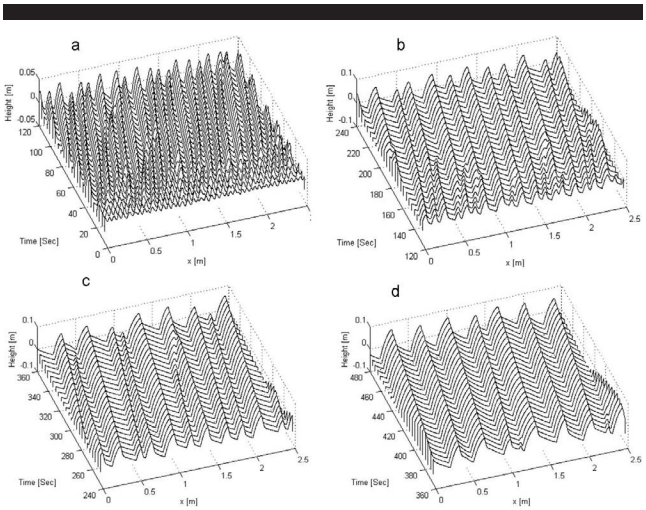


Figure 6. Ripples evolution calculated from the model equation (Equations 7 and 8) during the first 8 min. At the initial stage (panel a), the coarsening process is fast because there are many merging events where small ripples merge and form larger ripples. This process slows down at later times (panel b, c, d). After 24 min (not shown in the figure), the wavelength is 41.67 cm, and the mean height is 12.83 cm. Parameters: $b = 0.5$ m, $a = 0.01$ m, $\sigma = 0.0625$ m, and the other parameters as in Figure 5.

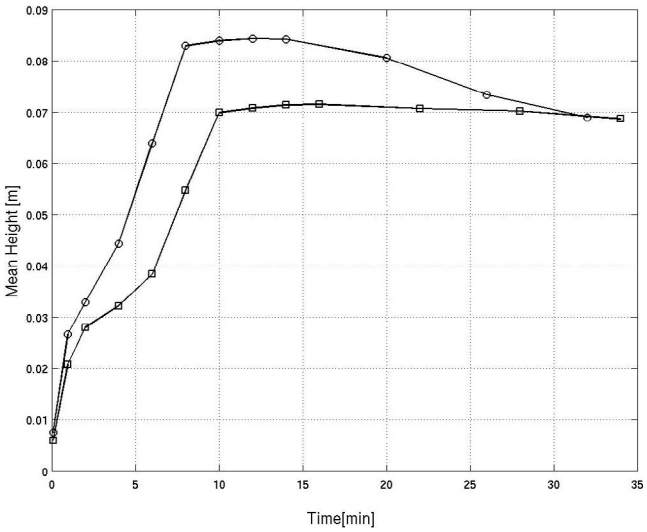


Figure 7. Ripple height *vs.* time plots for $\mu_s = 0.4$ (circles) and $\mu_s = 0.2$ (squares). After an initial linear growth, ripple height growth decreases, with the smaller $\mu_s$ having the higher ripples. The coarsening process for $\mu_s = 0.2$ after 15 min is characterized by a decrease in height because of the disappearance of some short wavelength ripples, as can be seen in Figure 5.

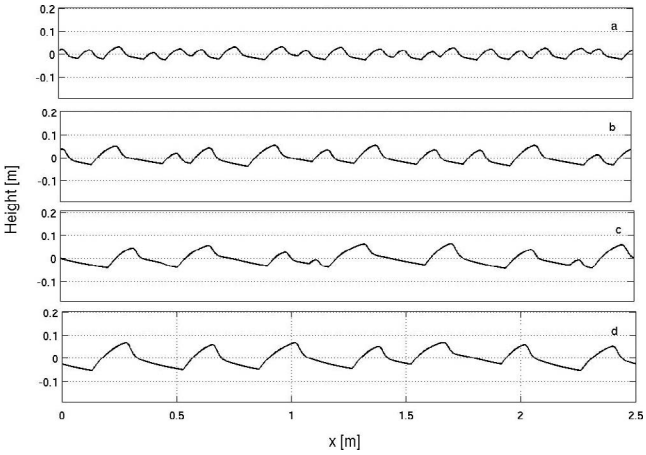


Figure 8. Ripple profiles at 2, 4, 6, and 8 min (a, b, c, d) for larger value of mean saltation jump ($b = 0.5$ m). The mean wavelength after 8 min is 35.71 cm, and the mean height is 10.2 cm, larger than that in the former simulations (Figures 4 and 5). Other parameters are: $a = 0.01$ m, $\sigma = 0.0625$ m, $\mu_r = 0.4$, $\delta = 27$, $\varphi = 10^0$, $\mu_s = 0.2$, $n_p = 1$.

height because some small ripples start to disappear, as can be seen in Figure 5.

Figure 8 shows the ripple profile at different times for a larger value of mean saltation length ($b = 0.5$ m). The mean wavelength after 8 min is 35.71 cm, and the mean height is 10.2 cm, larger than in the former simulations. The larger value of $b$ can be related to stronger winds, since the model predicts that megaripple height and spacing in such cases will be larger.

## DISCUSSION

Modeling of aeolian megaripple formation is complicated because it is necessary to account for the interaction of a variety of physical processes that are not completely understood and also because of the lack of accurate field experiments. The model presented here assumes that the bed is composed of two grain sizes, where the coarse grains undergo reptation due to energy imparted to the bed by the fine saltation particles. The model takes into account spatial variations of fine-particle saltation flux but does not account for the specific segregation mechanism of the bed, which is very important for megaripple formation. It also assumes constant flow over the bed form, which is probably altered above undulated surface (Anderson, 1990). Despite the crude simplifications taken on, the model succeeds in capturing the coarsening mechanism of the megaripples (*i.e.,* a significant increase in the wavelength), which are shown to start developing as normal ripples that subsequently coarsen via coalescence. The smaller, faster-moving ripples overtake larger, slower-moving ripples, resulting in increased size and spacing. Merging can be viewed as a selection process leading to the production of bed forms with similar-sized ripples; hence, the migration rate halts once the megaripples have attained identical sizes. The proposed model is two dimensional, and for actual three-dimensional megaripples, other types of merging interactions take place, such as defect migration or lateral linking, as is observed in normal ripples (Yizhaq, Balmforth, and Provenzale, 2004).

The final wavelength is not simply correlated to the mean saltation length, but it develops through interactions between ripples of different sizes. Larger wavelengths probably reflect longer development times and stronger winds. This is a common behavior of bed forms in different environments, such as ripples and dunes in rivers, oceans, and deserts (Werner, 1999). The megaripple system exhibits a self-organization behavior, where ordered spatio-temporal structures spontaneously emerge (Anderson, 1990; Kocurek and Ewing, 2005; Werner, 1995). The determining factor for megaripple wavelength is still open. There are two main theories. The first one (Murray, 2005) is that the large wavelength is due to the coarsening process, *i.e.,* the large wavelength of megaripples reflects the longer time during which the patterns have been developing through interactions between smaller ripples. According to this hypothesis, the linear stability analysis has to show that only modes that are related to normal ripples are unstable. The second hypothesis, which is presented here, suggests that there are two instabilities from the beginning: the larger wavelength corresponds to megaripples, and the smaller corresponds to normal ripples. In this scenario, large wavelengths of megaripples reflect both the larger unstable mode growth and also the increase through interactions between individual bed forms. Only, field experiments can determine which one of these hypotheses is correct.

Advancing the theory of megaripples will require verification via field and wind tunnel experiments. In the field, a well-documented experiment like the one conducted by Murray in the Western Sahara (Murray, 2005) with additional measurements of saltation and reptation fluxes (*cf.* Jerol-


Figure 9. Preliminary results of field experiments done at Nahal Kasuy dune field in the Southern Negev, Israel. (a) The initial flattened plot (5 m × 5 m) of megaripples. (b) The plot after 62 d. There is no clear indication for the development of megaripples. The bed is covered with normal megaripples. (c) The bed after 75 d. (d) The bed after 102 d is covered only by normal ripples.

mack *et al.,* 2006) should be able to test the common assumption that megaripples develop through the primarily saltative movements of the fine grains and the exclusive reptation of the coarse grains. Figure 9 shows our preliminary results of a field experiment that is still running at Nahal Kisui, southern Negev, Israel. This area is characterized by megaripples (wavelength 75 cm, height 10 cm). The figure shows the temporal evolution of a flattened bed over 102 d. After this period, the flattened area is covered only with normal ripples; thus, the process of megaripple formation may be quite slow in areas where the winds are not strong enough and their directional variability is high. We also observed that, during a strong storm, the megaripples in this dune field migrated downwind with a velocity of 1 cm/h. Using a portable wind tunnel in the field can be very useful in accelerating the development of the megaripples, and it will enable accurate measurements in a reasonable time.

Wind tunnel experiments could help investigate megaripple evolution in sands with different bimodal grain-size distributions and different wind speeds. Particularly, such studies could determine the minimal sorting index required for megaripple development and its dependence on the ratio of coarse to fine grain diameters. In such experiments, wind velocity will be varied from just above the saltation threshold for the finest grained sands to a value below the threshold for the coarsest sand, ensuring the saltation of fine particles alone.

However, it is clear that understanding of the long-term development of huge megaripples such those in the Carachi Pampa, Argentina (Milana, 2005), can be effectively achieved only via mathematical modeling. Because years and maybe decades are required for natural huge megaripple formation, field study is an impractical way of monitoring the long-term development of these natural bed forms or of evaluating the long-term effect of environmental changes on these systems. New mathematical models will have to include additional factors, such as the sorting mechanism, which will make calculations more time consuming. However, with the design of more efficient numerical codes, supercomputers should be able to number-crunch these advanced models of megaripple development over large space domains and extended periods of time.

## ACKNOWLEDGMENTS

I wish to thank Dr. Antonello Provenzale, Prof. Brad Murray, and Prof. Haim Tsoar for helpful discussion and Dr. Andreas Bass for reviewing this manuscript.

## LITERATURE CITED

Anderson, R.S., 1987. A theoretical model for aeolian impact ripples. *Sedimentology,* 34, 943–956.

Anderson, R.S., 1990. Eolian ripples as example of self-organization in geomorphological systems. *Earth-Science Reviews,* 29, 77–96.

Anderson, R.S. and Bunas, K.L., 1993. Grain size segregation and stratigraphy in aeolian ripples modeled with cellular automation. *Nature,* 365, 740–743.

Anderson, R.S. and Haff, P.K., 1988. Simulation of eolian saltation. *Science,* 241, 820–823.

Anderson, R.S. and Sørensen, M., 1991. A review of recent progress in our understanding of aeolian sediment transport. *Acta Mechanica (Suppl),* 1, 1–19.

Andreotti, B.; Claudin, P., and Pouliquen, O., 2006. Aeolian sand ripples: experimental study of fully developed states. *Physical Review Letters,* 96, Art. No. 028001.

Bagnold, R.A., 1941. *The Physics of Blown Sand and Desert Dunes.* London: Methuen.

Edgett, K.S., 2001. Observation regarding small eolian dunes and large ripples on Mars. Abstract 178-0, *Geological Society of America Abstracts with Programs, 33*(6).

El-Baz, F., 1986. The formation and motion of dunes and sand seas. *In:* El-Baz, F. and Hassan, M.H.A. (eds.), *Physics of Desertification.* Dordrecht: Martinus Hijhoff Publication, pp. 78–79.

Ellwood, J.M.; Evans, P.D., and Wilson, I.G., 1975. Small scale aeolian bedforms. *Journal of Sedimentary Petrology,* 45, 554–561.

Fausett, L.V., 1999. *Applied Numerical Analysis Using Matlab®*. Upper Saddle River, New Jersey: Prentice Hall.

Fryberger, S.G.; Hesp, P., and Hastings, K., 1992. Aeolian granule deposits, Namibia. *Sedimentology,* 39, 319–331.

Greeley, R.; Bridges, N.T.; Kuzmin, R.O., and Laity, J.E., 2002. Terrestrial analogs to wind-related features at the Viking and Pathfinder landing sites on Mars. *Journal of Geophysical Research–Planets,* 107(E1), Art. No. 5005 JAN 25 2002.

Jerolmack, D.J.; Mohrig, D.; Grotzinger, J.P.; Fike, D., and Watters, W.A., 2006. Spatial grain size sorting in eolian ripples and estimation of wind conditions on planetary surfaces: application to Meridiani Planum, Mars. *Journal of Geophysical Research–Planets,* 111(E5), Art. No. E12S02.

Jimenez, J.A.; Maia, L.P.; Serra, J., and Morais, J., 1999. Aeolian dune migration along the Cearà coast, north-eastern Brazil. *Sedimentology,* 46, 689–701.

Kocurek, G. and Ewing, R.C., 2005. Aeolian dune field self-organization—implications for the simple versus complex dune-field patterns. *Geomorphology,* 72, 94–105.

Milana, J.P., 2005. Unique gravelly dunes at the windiest place of the world: a natural laboratory for wind-driven catastrophes. *In: Holocene Environmental Catastrophes in South America: From the Lowlands to the Andes.* Miramar, Argentina: Laguna Mar Chiquita.

Misbah, C. and Valance, A., 2003. Sand ripples dynamics in the case of out-of-equilibrium aeolian regimes. *The European Physical Journal. E,* 12, 523–529.

Mountney, N.G. and Russell, A.J., 2004. Sedimentology of cold-cli-

mate aeolian sandsheet deposits in the Askja region of northeast Iceland. *Sedimentology,* 166, 223–244.
Murray, A.B., 2002. Seeking explanation affects numerical modeling strategies. *Eos, Transactions, American Geophysical Union,* 83, 418–419.
Murray, A.B., 2005. Bedform pattern evolution in two horizontal dimensions: extreme wavelength increases with mixed grain sizes. *Geophysical Research Abstracts,* 7, Art. No. 01859.
Nishimori, H. and Ouchi, N.B., 1993. Formation of ripple patterns and dunes by wind-blown sand. *Physical Review Letters,* 71, 197–201.
Ouchi, N.B. and Nishimori, H., 1995. Modeling of wind-blown sand using cellular automata. *Physical Review E,* 52, 5877–5880.
Prigozhin, L., 1999. Nonlinear dynamics of aeolian sand ripples. *Physical Review E,* 60, 729–733.
Rubin, D.M., 2006. Ripple effect: unforeseen applications of sand studies. *Eos, Transactions, American Geophysical Union,* 87(30), 293–297.
Sakamoto-Arnold, C.M., 1988. Eolian features produced by the December 1977 windstorm Southern San Joaquin Valley, California. *Journal of Geology,* 89, 129–137.
Saqqa, W. and Atallah, M., 2004. Characterization of the aeolian terrain facies in Wadi Araba Desert, southwestern Jordan. *Geomorphology,* 62, 63–87.
Sarre, R.D. and Chancey, C.C., 1990. Size segregation during aeolian saltation on sand dunes. *Sedimentology,* 37, 357–365.
Sharp, R.P., 1963. Wind ripples. *Journal of Geology,* 71, 617–636.
Tsoar, H., 1990. Grain-size characteristics of wind ripples on a desert seif dune. *Geography Research Forum,* 10, 37–50.
Walker, D.J., 1981. An Experimental Study of Wind Ripples. Cambridge, Massachusetts: Massachusetts Institute of Technology, M.Sc. thesis.
Werner, B.T., 1995. Eolian dunes. Computer simulations and attractor interpretation. *Geology,* 23, 1107–1110.
Werner, B.T., 1999. Complexity in natural landform patterns. *Science,* 24, 102–104.
Williams, S.H.; Zimbelman, J.R., and Ward, A.W., 2002. Large ripples on Earth and Mars. *Lunar and Planetary Science,* XXXIII, 1508.pdf.
Wilson, S.A.; Zimbelman, J.R., and Williams, S.H., 2003. Large aeolian ripples: extrapolations from Earth to Mars. *Lunar and Planetary Science,* XXXIV, 1862.pdf.
Yizhaq, H., 2004. A simple model of aeolian megaripples. *Physica A,* 338, 211–217.
Yizhaq, H., 2005. A mathematical model for aeolian megaripples on Mars. *Physica A,* 357, 57–63.
Yizhaq, H.; Balmforth, N.J., and Provenzale, A., 2004. Blown by wind: nonlinear dynamics of aeolian sand ripples. *Physica D,* 195, 207–228.